

LETTER

2-dimensional polar metals: a low-frequency Raman scattering study

To cite this article: Maxwell T Wetherington et al 2021 2D Mater. 8 041003

View the article online for updates and enhancements.

You may also like

Kanodia et al.

Mahadevan et al.

- NEID Rossiter–McLaughlin Measurement of TOI-1268b: A Young Warm Saturn Aligned with Its Cool Host Star Jiayin Dong, Chelsea X. Huang, George Zhou et al.
- GJ 3929: High-precision Photometric and <u>Doppler Characterization of an Exo-Venus</u> <u>and Its Hot, Mini-Neptune-mass</u> <u>Companion</u> Corey Beard, Paul Robertson, Shubham
- Observing the Sun as a Star: Design and Early Results from the NEID Solar Feed Andrea S. J. Lin, Andrew Monson, Suvrath

2D Materials



RECEIVED 8 May 2021

REVISED

14 August 2021

ACCEPTED FOR PUBLICATION 29 August 2021

PUBLISHED 16 September 2021

LETTER

2-dimensional polar metals: a low-frequency Raman scattering study

Maxwell T Wetherington^{1,2,*}, Furkan Turker², Timothy Bowen^{2,4}, Alexander Vera^{2,4}, Siavash Rajabpour^{2,5}, Natalie Briggs², Shruti Subramanian², Ashley Maloney⁶ and Joshua A Robinson^{1,2,3,4,7,*}

- Materials Research Institute, The Pennsylvania State University, University Park, PA, United States of America
- Department of Materials Science and Engineering, The Pennsylvania State University, University Park, PA, United States of America
- Center for 2-Dimensional and Layered Materials, The Pennsylvania State University, University Park, PA, United States of America
- Center for Nanoscale Science, The Pennsylvania State University, University Park, PA, United States of America
- ⁵ Chemical Engineering, The Pennsylvania State University, University Park, PA, United States of America
- ⁶ Physical Electronics, Chanhassen, MN, United States of America
- ⁷ Center for Atomically Thin Multifunctional Coatings, The Pennsylvania State University, University Park, PA, United States of America
- * Authors to whom any correspondence should be addressed.

E-mail: maxwell.wetherington@psu.edu and jrobinson@psu.edu

Keywords: epitaxial graphene, gallium, silver, lead, bismuth, copper, indium

Supplementary material for this article is available online

Abstract

The intercalation of a molecule or ion in a layered structure is key to enhancing energy storage, material conductivity, intercalant structural ordering, and the formation of two-dimensional (2D) superconducting states. The process of intercalation modifies the vibrational energy of the host, which can be monitored non-invasively by Raman spectroscopy. However, the detected Raman spectral shifts may originate from a variety of phenomena, generally making the technique an indirect means of identifying intercalation success. Here, we discuss newly discovered low-frequency (LF) ($<100~\rm cm^{-1}$) Raman features due to the formation of unique 2D polar metals (Ag, Cu, Pb, Bi, Ga, In) or metal alloys (In_xGa_{1-x}) intercalated at an epitaxial graphene (EG)/silicon carbide (SiC) interface and demonstrate that 2D-Ag and 2D-Ga can have spatially distinct phases with their own unique Raman responses. Additionally, we establish that the 2D-Ga exhibits a structural evolution as a function of temperature, independent of the SiC and EG, that can lead to nucleation of secondary phases. The newly identified LF Raman responses discussed here lay the foundation for rapid, direct, and spatially resolved evaluation of 2D polar metals in ambient.

Graphene catalyzed the age of 2D materials [1], however many other examples of atomically thin mono-element films pre-date graphene, existing at the metal-semiconductor interface—a key area of research for the development of many electronic devices [2]. However, the characterization of the monolayer metal-bulk semiconductor interface is generally limited to ultra-high vacuum (UHV) techniques due to rapid oxidation of the metal surface when exposed to ambient conditions [2]. Recently, with the advent of epitaxial graphene (EG) intercalation [3, 4] and subsequent development of confinement heteroepitaxy (CHet) [5], an atomicallythin (2D) metal can be automatically passivated by graphene and remain air-stable for >9 months [5]. The bonding character of the metal at this EG–SiC

interface is anisotropic, forming a covalent bond to the silicon and a weak van der Waals interaction with the graphene, which results in a noncentrosymmetric structure [5]. It has been determined that this axial symmetry breaking in the metal helps to generate the largest second-order susceptibility reported for metals (\sim 10 nm V⁻¹) [6] as well as higher $T_{\rm c}$ superconductors [5] compared to the bulk counterparts. The presence of the graphene capping layer helps to preserve these exotic states while also providing direct optical access to the metal layer outside of UHV.

Raman spectroscopy is a standard optical characterization technique for 2D materials [7]; however, analysis of mono-element metals or metal alloys via Raman spectroscopy is limited in comparison. There

are only a few examples of Raman scattering from bulk or surface phonons in mono-elemental transition metals [8–11]. In each case, the signal is either weak due to the skin depth of the metal that modulates the electronic susceptibility [12], or is only detected in UHV conditions due to oxygen sensitivity of the metal surface [11]. Recently, Raman scattering was found to occur as a result of electronphonon induced intraband electronic excitations in bulk metals at room temperature [13]. This electronic Raman scattering is dependent on the Fermi velocity of the metal and often results in spectroscopic features with full-width at half maximum (FWHM) values of 1000 cm⁻¹, which can be confused for fluorescence, except the peak position is independent of excitation source, confirming that it is a Raman shift [13]. Contrary to the electronic Raman scattering studies of metals, superconductor and semiconductor electronic Raman scattering is well established [14]. One of the earliest semiconductor materials identified to demonstrate electronic Raman scattering is 6H-SiC [15], the SiC polytype utilized in this work for epitaxial growth of graphene. The electronic Raman scattering in n-type SiC due to interband excitations from shallow donors is dependent on the unique valley-orbit split 1 s ground state found in each SiC polytype (4H, 6H, 15R).

Low-frequency (LF) Raman (defined <100 cm⁻¹) spectroscopy enables the characterization of inelastically scattered light from correlated electrons by probing the shallow donor/acceptor states in a material [14]. LF Raman also provides versatile information for layered materials based on rigid interlayer shear/breathing phonon modes [16]. These interlayer phonon modes enable the identification of layer thickness, stacking orientation, and the formation of Van Hove singularities in graphene [17] and other related layered materials [18]. The LF Raman (figure 1(a)) at various CHet synthesis stages demonstrate that only a weak band at -25 cm^{-1} exists in the semi-insulating 6H-SiC (<10¹⁶ cm⁻³ carrier concentration), multi-layer EG and hydrogen intercalated EG (referred to as quasi-freestanding EG or QFEGH). Because all Raman Stokes energy shifts have an equal but opposite anti-Stokes energy shift, this feature is assigned as an artifact from our 532 nm laser. We note that there are no interlayer phonon modes in EG (figure 1(a)). This may be due to azimuthal disorder beyond the first layer of graphene grown epitaxially on SiC (0001) (C-face) due to rotational stacking faults [19] or the dynamic change in strain for each subsequent layer [20] on SiC (0001) (Si-face).

New LF Raman features appear only after metal intercalation and are thus referenced as metal low frequency features (MLFF). The gallium (Ga) intercalated EG (QFEG_{Ga}) exhibit intense bands at 26 ± 1.3 cm⁻¹ and 54 ± 2.1 cm⁻¹ with a descending background from low-to-high wavenumbers. As

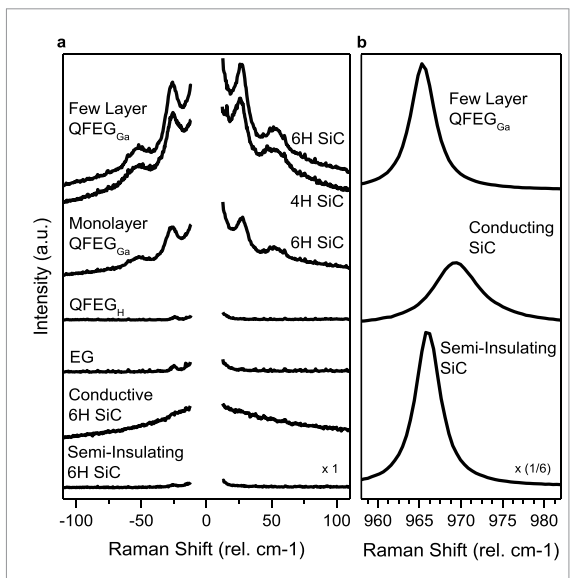


Figure 1. (a) Low frequency Raman (532 nm laser) acquired at various stages of the CHet process, with spectra normalized to the 6H-SiC folded transverse acoustic (FTA) mode at 150 cm $^{-1}$, reveals that only after metal intercalation do the additional modes appear at $26\pm1.3~{\rm cm}^{-1}$ and $54\pm2.1~{\rm cm}^{-1}$. Additionally, (b) the intercalation of the 2D metal does not alter the position of the SiC LOPC mode, indicating no measurable change in the SiC carrier concentration as a result of CHet.

seen in figure 1(a), the general peak profile of the QFEG_{Ga} is independent of the EG layer thickness and SiC polytype, indicating that this is not an interlayer mode unique to EG, nor electronic Raman scattering from interband excitations in the SiC. However, there is a subtle difference in the MLFF relative intensity for monolayer QFEGGa and bilayer QFEGGa. This is likely related to the concentration of oxygen present in the intercalated Ga, which leads to quenching of the LF Raman response (see supporting info available online at stacks.iop.org/2DM/8/041003/mmedia), as has been found by Akemann et al [11]. While gallium oxide does have a Raman response at >200 cm⁻¹ [21], the weak signal is not detected in our 2D metal structure. Another feature in the QFEGGa LF spectra is the descending background, which also exists in conductive SiC (>10¹⁷ electrons cm⁻³ carrier concentration). As carrier concentration of SiC is increased, this background appears as a result of a continuum band due to intraband transitions [15, 22]. Additionally, when an increase in carrier concentration in SiC occurs, it induces a positive shift and damping of the longitudinal phonon plasmon coupled (LOPC) mode [23] and the Fano interference in the folded transverse acoustic (FTA) mode [24]. Therefore, if the carrier concentration of the semi-insulating SiC substrate increased to $\geq 10^{17}$ cm⁻³ due to Ga intercalation, the LOPC peak would shift $\geq +1$ cm⁻¹ compared to semi-insulating 6H-SiC [23]. As shown in figure 1(b), the LOPC peak in semi-insulating 6H-SiC (966.0 cm^{-1}) and QFEG_{Ga} (965.8 cm^{-1}) is unchanged within our measurement accuracy,

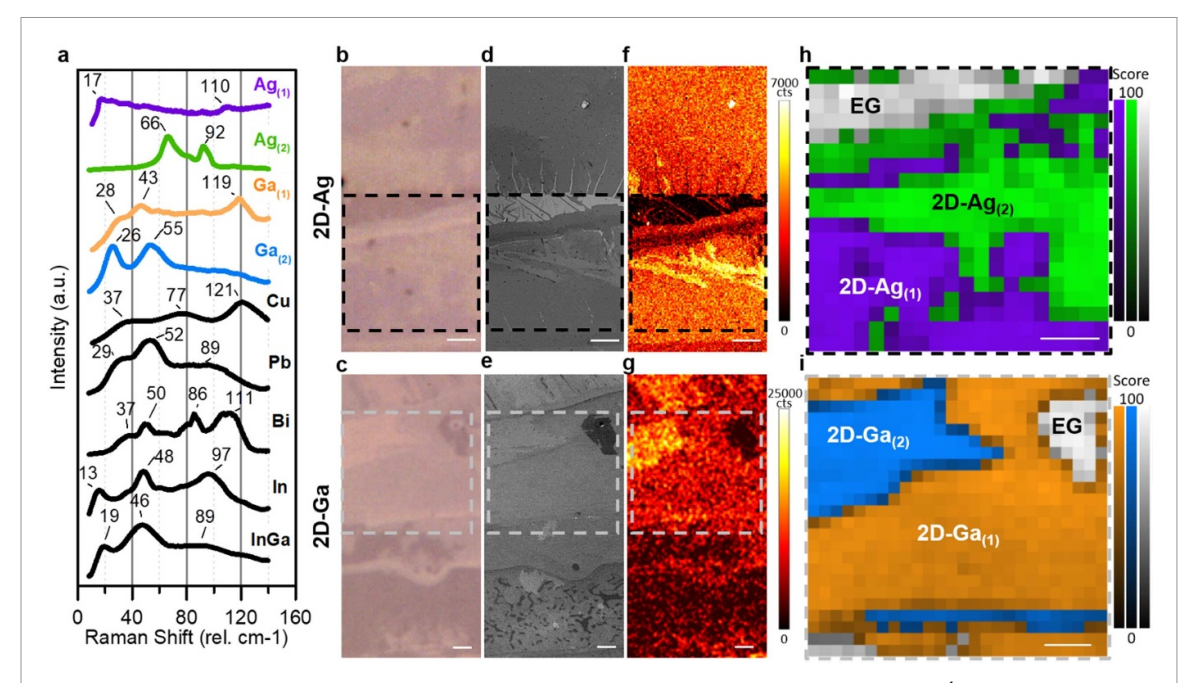


Figure 2. (a) Each 2D-metal exhibits a unique MLFF (labeled peak position standard deviation $\leq 2.5 \text{ cm}^{-1}$), with both 2D-Ag and 2D-Ga showing two spatially distinct responses. Contrast in reflected light optical micrographs ((b), (c)), secondary electron SEM ((d), (e)) and Auger electron spectroscopy (AES) maps of Ag1 359 eV photoelectron (f) and Ga1 1069 eV photoelectron (g) corresponds with the unique phases identified in Raman map analysis of the 2D-Ag (h) and 2D-Ga (i), respectively. The bright region in the AES maps indicates a higher signal and therefore higher concentration of the metal. These regions of higher concentration from Auger match 2D-Ag₍₂₎ in (h) and 2D-Ga₍₂₎ in (i). Each pixel in the Raman maps ((h), (i)) represent an acquired spectrum analyzed via multivariate curve resolution (MCR), where the pixel color is chosen based on the loading with the highest score. The loadings for the maps (purple/green; orange/blue) are color coded in (a). The scale bar in all images ((b)–(i)) is 2 μ m.

suggesting no detectable doping of the SiC due to intercalation. Therefore, the LF background feature in the QFEG_{Ga} sample is a direct response of the intercalated metal. Furthermore, the QFEG_{Ga} MLFF is unique from the measured response of bulk gallium [25] and gallium clusters embedded in an Ar⁺ matrix [26], likely due to the polar structure formed at this interface [5]. To help clarify this differentiation in structure and spectral response, the metal intercalated QFEG region is identified by the 2D-metal (2D-Ga, 2D-Ag, etc) intercalant.

Each metal intercalant exhibits a MLFF that is a unique spectral fingerprint, enabling rapid identification of the 2D-metal. As evidenced by the Stokes shift spectra (figure 2(a)) for each metal intercalant after Bose-Einstein population correction [27], no two metals exhibit the same MLFF. Additionally, two distinct MLFF exist for 2D-Ag and 2D-Ga. Often, 2D-metal samples exhibit variation in optical micrograph contrast (OM, figures 2(b) and (c)), scanning electron microscopy (SEM, figures 2(d) and (e)), and Auger electron spectroscopy maps (AES, figures 2(f) and (g)), indicating different concentrations of metal in the corresponding regions. Raman maps of 2D-Ag (figure 2(h)) and 2D-Ga (figure 2(i)) match these sample specific variations in OM, SEM, and AES, validating that Raman mapping of the 2D-metals provides a rapid and direct means for identifying location specific phases of the metals. Previous TEM analysis demonstrates Ag and Ga intercalation can

result in 1–4 atomic layers and occasionally 4+ atomic layers [5]; however, only two distinct MLFFs are identified (based on dozens of 2D-Ag and 2D-Ga samples). Therefore, the MLFF is likely measuring a distinction in structure that occurs after some threshold thickness or concentration (e.g. intralayer packing) of the Ag and Ga intercalation. Characterizing this structural difference is challenging and is a continued effort in our research.

The MLFF response measured for each 2D metal is unique from their respective bulk metal; however, some shared similarities exist for 2D-Ag, 2D-Cu and 2D-Bi. Cryocondensed Ag and Cu exhibit peaks at 65, 110, and 170 cm⁻¹ for Ag and 112, 157, and 222 cm⁻¹ for Cu [11]. The feature identified at 65 cm⁻¹ in the cryocondensed Ag film, which also appears in 2D-Ag in this study (65 \pm 0.4 cm⁻¹), was assigned to a surface acoustic wave (or Rayleigh wave) that crosses the M & K point of the Ag(111) Brillouin zone [11]. Additionally, Helium time-of-flight spectroscopy indicates Ag(111) also has surface longitudinal resonance phonons that cross the M & K point of the Brillouin zone at 81 and 97 cm⁻¹ [28], respectively, similar to the 83 \pm 0.6 and 92 \pm 0.4 cm $^{-1}$ peaks in 2D-Ag₍₂₎. It is possible these surface longitudinal features were not resolved previously due to film roughness consisting of multiple small facets, including (111), (110), and (100) faces, all contributing to the inelastic scattering [11]. Whereas the atomically-smooth, 2D-metals in this study results in



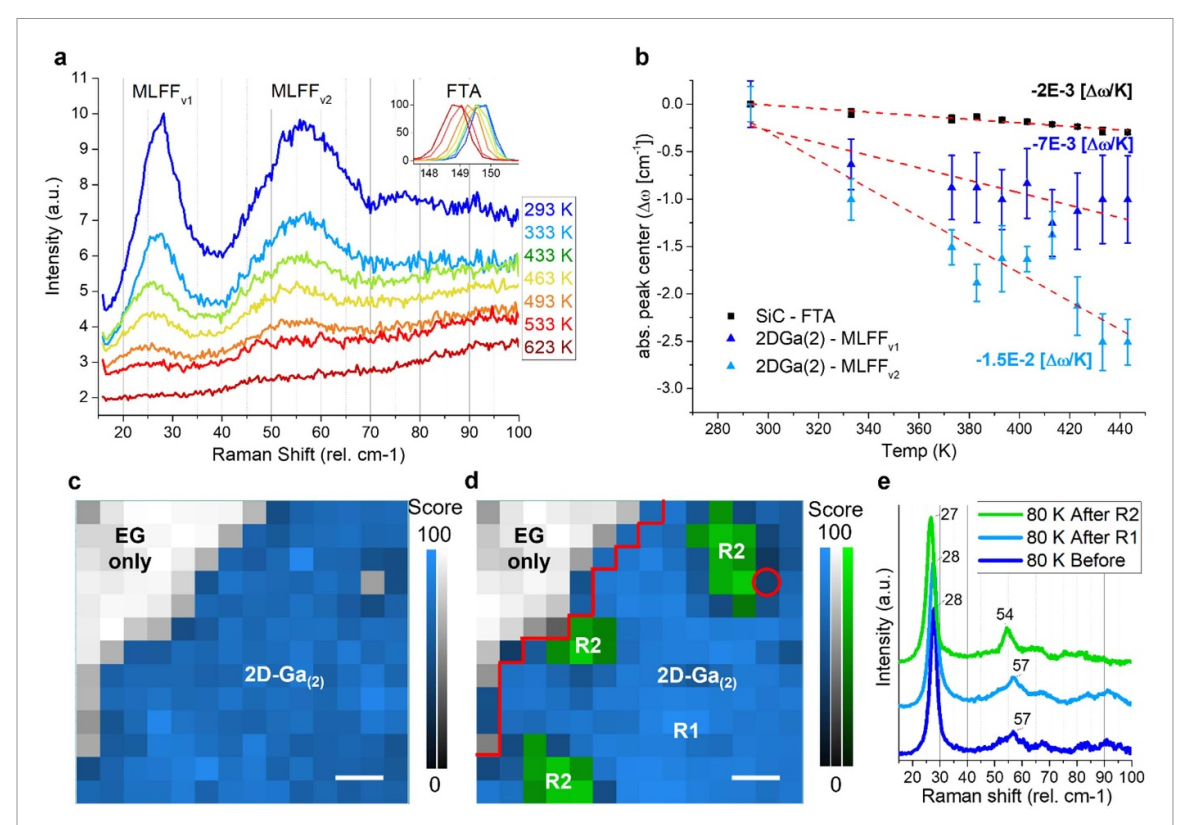


Figure 3. (a) Temperature (293 K–623 K) dependent Raman response (633 nm laser, $50 \times /\text{NA}0.5$, spatial resolution $<1~\mu\text{m}$) of 2D-Ga₍₂₎ demonstrates an evolution in MLFF_{v1} and MLFF_{v2} with increasing temperature (inset is the SiC FTA response), where (b) plotting the peak positions as a function of temperature indicate the 2D-Ga₍₂₎ exhibits a much stronger temperature dependence than SiC. Furthermore, Raman maps (MCR analysis) of the 2D-Ga₍₂₎ at 80 K before (c) and after (d) heating the sample to 623 K reveal that a new phase appears ((d), green) after cooling back down to 80 K. This second phase (R2) appears near the edges of the original 2D-Ga₍₂₎ structure, with a shift in both MLFF_{v1} and MLFF_{v2} (e). The red line in (d) is the outline of the 2D-Ga₍₂₎ region from (c). Scale bar in ((c), (d)) is 4 μ m.

discrete structures with a domain size on the order of microns, resulting in a phase-dependent Raman response (figure 2(h)), where 2D-Ag₍₂₎ could possibly correspond to Ag(111) and the 2D-Ag(1) matching Ag(100) at 110 cm⁻¹ [11]. However, the strongest response detected in 2D-Ag₍₁₎ is at 17 \pm 1.0 cm⁻¹, which does not exist in the reported Ag(100) structure [11]. The agreement between the cryocondensed Cu film Raman response and the 2D-Cu is not as clear, with only a close correlation between the feature identified at \sim 112 cm⁻¹ and 121 \pm 1.0 cm⁻¹, respectively. Helium time-of-flight spectra of Cu(111) reveals that the Rayleigh wave crosses the M & K point of the Brillouin zone at 108 cm⁻¹ and 113 cm⁻¹, matching the cryocondensed Cu film [28]. However, higher index Cu structures result in folded surface phonon modes that cross the Γ point of the Brillouin zone at lower frequencies than Cu(111) [29]. Lastly, the 2D-Bi measured Raman response does show a close correlation with recently measured Bi-III in a high pressure Raman scattering study [30]. However, the signal at \sim 108 cm⁻¹ identified in their phonon density of states as the out-of-plane component is stronger in our measurement than the system tested by Zhao et al possibly because the lower dimensionality of the 2D-Bi within the QFEG-SiC gallery enhances the out-of-plane motion [30]. Once the atomic structure of these 2D metals is confirmed, a more thorough analysis on the phonon assignments can be provided. This would be most useful in the analysis of the Pb, In and In_xGa_{1-x} alloy system, for which there is no known Raman reported prior to this publication.

Temperature dependence of the 2D-metal MLFF is uniquely different from SiC and QFEG. There is a monotonic decrease in position/intensity and increase in FWHM of the 2D-Ga(2) peaks from 290 K to \sim 600 K (figure 3), when signal can no longer be detected. The decrease in phonon frequency with increasing temperature is typical for materials with a positive coefficient of thermal expansion, and is due to an anharmonic potential of the vibrational mode [31]. The SiC Raman bands follow the same trend, however, the shift in the FTA peak position as a function of temperature for SiC $(-0.002 \text{ cm}^{-1} \text{ K}^{-1})$ [32] is less than that measured for 2D-Ga₍₂₎ MLFF_{v1} $(-0.007 \text{ cm}^{-1} \text{ K}^{-1})$ and $MLFF_{v2}$ (-0.015 cm⁻¹ K⁻¹). The temperature induced line-shift in SiC decreases as the wavenumber, ω_0 , of the respective phonon decreases, with a measured dispersive response of $C(\omega_{\rm o}) = -2 \times 10^{-5} \omega_{\rm o} + 0.002 \,{\rm cm}^{-1}$ [32]. If the detected MLFF originated from SiC, the MLFF would



have a positive temperature coefficient. This indicates that the spectral-structural dependence of the 2D metal is unique. If the temperature coefficient for the 2D metal is presumed to also show a linear dispersive response—limited to only two MLFFs for 2D-Ga₍₂₎, then $C(\omega_0) = -2 \times 10^{-4} \omega_0 + 0.0002 \text{ cm}^{-1}$. Once the origin of these modes is identified and the non-linear compression as a function of 2D metal thermal expansion is determined, these shifts can be equated to structural changes in the 2D metal. However, using this dispersive response of 2D metal Raman as a function of temperature, we can estimate that the expected dispersion for the G peak would be -0.3442 cm⁻¹ K⁻¹, which is $>10\times$ the measured value for QFEG [33], thus eliminating the possibility of the MLFF response coming from QFEG.

Mapping the Raman response before and after thermal cycling (figures 3(c) and (d)) provides insights into 2D metal diffusion and reconstruction at the QFEG-SiC interface. As noted previously, increasing the temperature reduces the MLFF intensity due to the ground vibrational state being depleted as energy in the system is increased [31]. However, the spectra in figures 3(a) and (e) compensates for thermal population of states by applying the Bose-Einstein correction. Therefore, the decrease in signal intensity may be assigned to increased disorder in the 2D metal structure. A comparison of the 2D-Ga₍₂₎ sample measured at 80 K before (figures 3(c) and (e)) and after (figures 3(d) and (e)) heating to 623 K, reveals that the 2D metal structure returns to its original state in most regions (R1) of the mapped sample; however, a 2nd region appears (R2) in multiple locations (green in figures 3(d) and (e)). Region R2 appears to nucleate at the edge of the original 2D-Ga₍₂₎ structure, with a higher tensile strain based on the red-shift of the phonons with respect to the original 2D-Ga₍₂₎ measured response at 80 K (figure 3(e)). In the upper-right quadrant of the Raman map (figures 3(c) and (d)), a location that was previously identified as 'EG only' now exhibits the R2 response, suggesting that the 2D-Ga metal has diffused into this location, forming QFEG_{Ga} with a Ga layer thickness greater than 2D- $Ga_{(1)}$ (see supporting info), and the structure is under tensile strain.

The ability to rapidly assess the presence, composition and structure of 2D-metals at the interface of QFEG-SiC at sub-micron scales, under ambient conditions, is a unique advantage of Raman spectroscopy. The temperature dependent spectral analysis of the 2D metal demonstrates that Raman is a direct approach to monitoring the stability and diffusion *in-situ*. Once a spectral-structural relationship is established for the 2D metals, this characterization method is poised to help understand other critical properties of the 2D metal, such as the strain, crystallinity, electron-phonon coupling, non-linear optical coefficients, and correlated electrons in the superconducting state.

Data availability statement

The data that support the findings of this study are available upon reasonable request from the authors.

Acknowledgments

This work was supported in part by Horiba Scientific, the Air Force Office of Scientific Research (FA9550-19-1-0295), the National Science Foundation (NSF) under DMR-2002651 and DMR-2011839 through the Penn State MRSEC—Center for Nanoscale Science, the 2D Crystal Consortium NSF Materials Innovation Platform under cooperative agreement DMR-1539916. We thank Horiba application scientists David Tuschel, Fran Adar, Bridget O'Donnell and Sergey Mamedov, the staff within the Materials Characterization Laboratory in the Materials Research Institute at The Pennsylvania State University, John Newman and Ben Schmidt from Physical Electronics for measurement assistance and fruitful discussions.

ORCID iD

Maxwell T Wetherington https://orcid.org/0000-0003-1958-1354

References

- [1] Novoselov K S *et al* 2004 Electric field effect in atomically thin carbon films *Science* **306** 666–9
- [2] Brillson L J 1982 The structure and properties of metal-semiconductor interfaces Surf. Sci. Rep. 2 123–326
- [3] Riedl C, Coletti C, Iwasaki T, Zakharov A A and Starke U 2009 Quasi-free-standing epitaxial graphene on SiC obtained by hydrogen intercalation *Phys. Rev. Lett.* 103 246804
- [4] Kubler L, Aït-Mansour K, Diani M, Dentel D, Bischoff J-L and Derivaz M 2005 Bidimensional intercalation of Ge between SiC(0001) and a heteroepitaxial graphite top layer *Phys. Rev.* B 72 115319
- [5] Briggs N et al 2020 Atomically thin half-van der Waals metals enabled by confinement heteroepitaxy Nat. Mater. 19 637–43
- [6] Steves M A et al 2020 Unexpected near-infrared to visible nonlinear optical properties from 2D polar metals Nano Lett. 20 8312–8
- [7] Paillet M, Parret R, Sauvajol J-L and Colomban P 2018 Graphene and related 2D materials: an overview of the Raman studies J. Raman Spectrosc. 49 8–12
- [8] Grant W B, Schulz H, Hüfner S and Pelzl J 1973 Investigation of k = 0 phonons in Bi, Cd, Mg, and Zn by Raman scattering Phys. Status Solidi b 60 331–40
- [9] Feldman D, Parker J and Ashkin M 1968 Raman scattering by optical modes of metals *Phys. Rev. Lett.* 21 607
- [10] Parker J H, Feldman D W and Ashkin M 1969 Raman Scattering by Optical Modes of Metals. In Light Scattering Spectra of Solids ed G B Wright (Berlin: Springer) pp 389–97
- [11] Akemann W, Otto A and Schober H R 1997 Raman scattering by bulk phonons in microcrystalline silver and copper via electronic surface excitations *Phys. Rev. Lett.* 79 5050–3
- [12] Mills D, Maradudi A A and Burstein E 1970 Theory of Raman effect in metals Ann. Phys. 56 504



- [13] Ponosov Y S and Streltsov S V 2012 Measurements of Raman scattering by electrons in metals: the effects of electron-phonon coupling *Phys. Rev.* B 86 045138
- [14] Devereaux T P and Hackl R 2007 Inelastic light scattering from correlated electrons *Rev. Mod. Phys.* **79** 175–233
- [15] Colwell P J and Klein M V 1972 Raman scattering from electronic excitations in n-type silicon carbide *Phys. Rev.* B 6 498–515
- [16] Zhang X, Tan Q-H, Wu J-B, Shi W and Tan P-H 2016 Review on the Raman spectroscopy of different types of layered materials *Nanoscale* 8 6435–50
- [17] Cong C and Yu T 2014 Enhanced ultra-low-frequency interlayer shear modes in folded graphene layers *Nat. Commun.* 5 4709
- [18] Lu X, Luo X, Zhang J, Quek S Y and Xiong Q 2016 Lattice vibrations and Raman scattering in two-dimensional layered materials beyond graphene *Nano Res*. 9 3559–97
- [19] Emtsev K V, Speck F, Seyller T, Ley L and Riley J D 2008 Interaction, growth, and ordering of epitaxial graphene on SiC{0001} surfaces: a comparative photoelectron spectroscopy study *Phys. Rev. B* 77 155303
- [20] Ferralis N, Maboudian R and Carraro C 2008 Evidence of structural strain in epitaxial graphene layers on 6H-SiC(0001) Phys. Rev. Lett. 101 156801
- [21] Zhao Y and Frost R L 2008 Raman spectroscopy and characterisation of α-gallium oxyhydroxide and β-gallium oxide nanorods J. Raman Spectrosc. 39 1494–501
- [22] Harima H, Hosoda T and Nakashima S 2000 Carrier density evaluation in P-type SiC by Raman scattering Mater. Sci. Forum 338–42 607–10
- [23] Nakashima S, Harima H, Ohtani N and Katsuno M 2004 Raman characterization of local electrical properties and

- growth process in modulation-doped 6H-SiC crystals *J. Appl. Phys.* **95** 3547–52
- [24] Mitani T, Nakashima S, Kojima K, Kato T and Okumura H 2012 Determination of carrier concentration by Fano interference of Raman scattering in heavily doped n-type 4H-SiC J. Appl. Phys. 112 043514
- [25] Creighton J A and Withnall R 2000 The Raman spectrum of gallium metal *Chem. Phys. Lett.* **326** 311–3
- [26] Himmel H J and Gaertner B 2004 Characterization of isolated Ga-2 molecules by resonance Raman spectroscopy and variations of Ga-Ga bonding *Chem. Eur. J.* 10 5936–41
- [27] Kauffmann T H, Kokanyan N and Fontana M D 2019 Use of stokes and anti-stokes Raman scattering for new applications J. Raman Spectrosc. 50 418–24
- [28] Harten U, Toennies J P and Wöll C 1985 Helium time-of-flight spectroscopy of surface-phonon dispersion curves of the noble metals *Faraday Discuss. Chem. Soc.* 80 137–49
- [29] Raouafi F, Barreteau C, Desjonquères M C and Spanjaard D 2002 The phonon spectra of low and high index surfaces of copper Surf. Sci. 507–510 748–53
- [30] Zhao Y, Clement S, Haines J and Viennois R 2020 Lattice dynamics study of elemental bismuth under high pressure J. Phys. Chem. C 124 26659–69
- [31] Lucazeau G 2003 Effect of pressure and temperature on Raman spectra of solids: anharmonicity J. Raman Spectrosc. 34 478–96
- [32] Bauer M, Gigler A M, Huber A J, Hillenbrand R and Stark R W 2009 Temperature-depending Raman line-shift of silicon carbide J. Raman Spectrosc. 40 1867–74
- [33] Tang X, Xu S and Wang X 2014 Corrugated epitaxial graphene/SiC interfaces: photon excitation and probing Nanoscale 6 8822–30